# Micromagnetic study of magnetization reversal in inhomogeneous permanent magnets

Zhi Yang(杨质), Yuanyuan Chen(陈源源), Weiqiang Liu(刘卫强)†, Yuqing Li(李玉卿), Liying Cong(丛利颖), Qiong Wu(吴琼), Hongguo Zhang(张红国), Qingmei Lu(路清梅), Dongtao Zhang(张东涛), and Ming Yue(岳明)‡

*Faculty of Materials and Manufacturing, Key Laboratory of Advanced Functional Materials (Ministry of Education), Beijing University of Technology, Beijing* 100124, *China*

(Received 10 July 2022; revised manuscript received 6 September 2022; accepted manuscript online 21 September 2022)

Macroscopic magnetic properties of magnets strongly depend on the magnetization process and the microstructure of the magnets. Complex materials such as hard-soft exchange-coupled magnets or just real technical materials with impurities and inhomogeneities exhibit complex magnetization behavior. Here we investigate the effects of size, volume fraction, and surroundings of inhomogeneities on the magnetic properties of an inhomogeneous magnetic material via micromagnetic simulations. The underlying magnetization reversal and coercivity mechanisms are revealed. Three different demagnetization characteristics corresponding to the exchange coupling phase, semi-coupled phase, and decoupled phase are found, depending on the size of inhomogeneities. In addition, the increase in the size of inhomogeneities leads to a transition of the coercivity mechanism from nucleation to pinning. This work could be useful for optimizing the magnetic properties of both exchange-coupled nanomagnets and inhomogeneous single-phase magnets.

**Keywords:** permanent magnets, micromagnetic simulation, exchange-coupling, multilayers

**PACS:** 75.78.Cd, 75.78.–n, 75.90.+w **DOI:** 10.1088/1674-1056/ac9359

## 1. Introduction

Currently, widely used high-performance permanent magnets are made from rare-earth transition metal intermetallic compounds such as Nd–Fe–B,[1,2] Sm–Co,[3–7] and Sm–Fe–N.[8] The macroscopic magnetic properties are not only dominated by the materials parameters of the main ferromagnetic component of the magnet but also highly dependent on the microstructure and the microscopic magnetization processes of the magnets.[9–11] Therefore, performance of permanent magnets can be supplemented and enhanced by microstructure modifications and manipulations, such as elemental substitution,[12] and grain boundary diffusion.[13] Noticeably, a great idea with real potential to significantly raise the record energy product is the oriented exchange-spring hard-soft nanocomposite magnet.[9,14,15] As compared to the ideally homogeneous magnetic materials which exhibit a relatively simple and well-understand magnetization behavior, the materials with complex microstructures, such as real technical materials with impurities and inhomogeneities or two-phase composites, exhibit a far more complex magnetization behavior.[16] Nucleation and pinning are the two main coercivity mechanisms of permanent magnets, and the permanent magnets are correspondingly classified into so-called nucleation-type and pinning-type materials. It has been stated in Brown's paradox[17] that the coercivity in all real magnets lies below the theoretically calculated anisotropy field due to the presence of inhomogeneities that are either unavoidable or specifically introduced into the magnet,[18] and they also play significant roles in adjusting the coercivity mechanism. Therefore, the knowledge of the magnetization reversal process and coercivity mechanism in such complex magnetic materials is of prime importance for an in-depth understanding of their magnetic properties in order to help for further improvements.

Extensive experiment works have been made to study the magnetization process by observing the domain structure through Lorentz transmission electron microscopy,[19] magnetic force microscopy,[20,21] or Bitter-pattern.[22] However, the techniques for visualizing domain structures depend on sensing the stray field outside the magnetic materials and beg the question of whether the domains observed at the surface are actually representative of the bulk. Therefore, direct experimental observation of the magnetization dynamics inside the permanent magnets is rather difficult.[18] Instead, micromagnetic simulation provides an important way to reveal the magnetization dynamics in permanent magnets.[23–25] Up to date, micromagnetic simulations[26–29] have been widely used to study the magnetization phenomena on the intermediate scale between the quantum mechanical scale of individual atoms and the macroscale, such as the dynamic response of a micromagnetic system and the characterization of 3D magnetization distribution.[9,30] By employing large-scale micromagnetic simulations, the effects of grain size,[31] grain shape,[32] and grain boundary phase[33] on the coercivity of Nd–Fe–B

†Corresponding author. E-mail: liuwq@bjut.edu.cn
‡Corresponding author. E-mail: yueming@bjut.edu.cn

© 2023 Chinese Physical Society and IOP Publishing Ltd 

permanent magnets were well investigated. Therein, the micromagnetic simulations provided a valuable tool to understand the magnetization reversal process and the coercivity mechanism of complex permanent magnetic materials.

In this work, magnetization reversal process of an inhomogeneous magnetic material is investigated by micromagnetic simulation on a multilayer structure, in which the soft-magnetic layers are used to represent the area with reduced coercivity compared to the bulk, due to impurities or atomic disorder, or an area consisting of a different material as found in the composite material. The micromagnetic model used in the present work is nevertheless complicated enough to exhibit and explain many of the phenomena related to magnetization reversal processes. Different demagnetization modes and coercivity mechanisms are found, depending on the size of the inhomogeneities. In addition, the effects of volume fraction and surroundings of the inhomogeneity on the magnetic properties are discussed. The micromagnetic approach introduced in the present work is fundamental enough to help to understand the magnetization behavior in both exchange-coupled nanomagnets and inhomogeneous single-phase magnets.

## 2. Simulated model and method

The magnetization distribution was simulated using the micromagnetic simulator OOMMF (Object Oriented MicroMagnetic Framework)[34] by dynamically solving the Landau–Lifshitz–Gillbert equation with a finite differences method.[35] The Gilbert damping parameter $\alpha = 0.5$ has been used to make a good balance between calculation precision and speed.[10] The schematic diagram of the micromagnetic model based on an *o-xyz* coordinate system is illustrated in Fig. 1. The soft magnetic layer enclosed with hard-magnetic layers was used to represent the inhomogeneity in the interior of the bulk magnets, while the soft-magnetic layer with only one side in contact with the hard-magnetic layer is used to represent the surface inhomogeneities. The superscripts h and s represent the hard-magnetic and soft-magnetic layers, respectively. As a result, the $t_h$ and $t_s$ denote the thickness of the hard-magnetic and soft-magnetic layers, respectively. The length and width of the multilayers are fixed at 300 nm. To investigate the effects of the size and the volume fraction of the inhomogeneity on the magnetic properties, we calculated the demagnetization curves of the multilayer structure with various layer thicknesses as detailed in the following section. The magnetic field (from 14 T to −14 T) is applied in the $z$-direction, and the easy axes of the hard-magnetic layers are assumed to be perpendicular to the layer plane. The simulation mesh size of 3 nm×3 nm×0.5 nm for $t_s = 1$ nm or $t_h = 1$ nm, and 3 nm×3 nm×1 nm for the others. Here we selected $SmCo_5$ and $Fe_{65}Co_{35}$ as the hard-magnetic phase and soft-magnetic phase, respectively, and the magnetic parameters including anisotropy $K_1$, saturation magnetization $M_s$, and exchange constant $A$ of $SmCo_5$[36] and $Fe_{65}Co_{35}$[18] are as follows: $K_1 = 17.2$ MJ·m$^{-3}$, $M_s = 0.86$ MA·m$^{-1}$, $A = 12$ pJ·m$^{-1}$ for the $SmCo_5$ alloy, and $K_1 = 0.02$ MJ·m$^{-3}$, $M_s = 1.95$ MA·m$^{-1}$, $A = 16.7$ pJ·m$^{-1}$ for the $Fe_{65}Co_{35}$ alloy. The guidelines revealed in the present work are not believed to be limited to the $SmCo_5$/$Fe_{65}Co_{35}$ magnets but could be applied to other permanent magnets with different constituent phases.

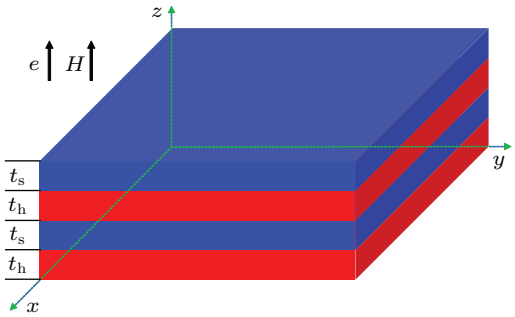



**Fig. 1.** Micromagnetic model for an inhomogeneous magnet consisting of soft and hard magnetic layers. The thicknesses of the soft-magnetic and hard-magnetic layers are denoted by $t_s$ and $t_h$, respectively. The applied field and easy axis of the hard-magnetic phase are parallel to the $z$-axis.

## 3. Results and discussion

The calculated demagnetization curves for different volume fractions of softmagnetic phase $V_s$ ($V_s = \frac{t_s}{t_s+t_h}$), with the soft-magnetic-phase thicknesses $t_s = 1$ nm, $t_s = 5$ nm, and $t_s = 10$ nm are shown in Figs. 2(a), 2(b), and 2(c), respectively. As can be seen from Fig. 2, the volume fraction of the soft magnetic phase highly influences the magnetic properties. The saturation magnetization $M_s$ is an intrinsic material property, which can be estimated from the equation $M_s = M_s^h \frac{t_h}{t_s+t_h} + M_s^s \frac{t_s}{t_s+t_h}$, where $M_s^h$ and $M_s^s$ are the saturation magnetization of the soft-magnetic phase and hard-magnetic phase, respectively. The saturation magnetization is decisive for the remanence $M_r$ and the maximum magnetic energy product $(BH)_{max}$.[37] It is clear from Fig. 2 that the demagnetization process for the case of $t_s = 1$ nm is different from the cases of $t_s = 5$ nm and $t_s = 10$ nm. As seen from Fig. 2(a), the remanence $M_r$ is approximately equal to $M_s$ when $t_s = 1$ nm and demagnetization curves show a good squareness which is called a rigid composite magnet.[23] On the contrary the $M_r$ lies below the $M_s$ when $t_s = 5$ nm (Fig. 2(b)), and the demagnetization process is clearly separated into two parts (i.e., the slightly decreasing magnetization at the lower applied field, and the jump at the higher applied field). This implies that the magnetization reversal is expected to start from the soft-magnetic phase prior to the magnetization of hard-magnetic phase switching. In the case of $t_s = 10$ nm (Fig. 2(c)), with the increase of $V_s$, the demagnetization curves collapse, resulting

in a significant decrease of coercivity $H_c$ (Fig. 2(c)). In addition, several jumps and steps appear in the demagnetization curves in the cases of $t_s = 5$ nm and $t_s = 10$ nm. The underlay magnetization reversal mechanism will be discussed later.

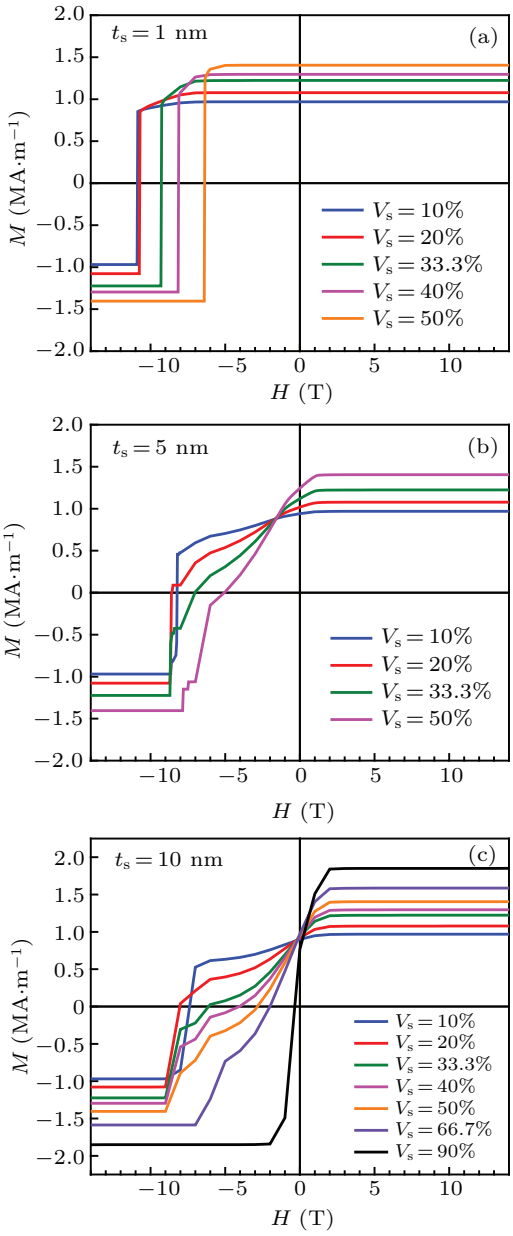



**Fig. 2.** The calculated demagnetization curves for different volume fractions of soft-magnetic phase $V_s$, with the soft-magnetic-phase thicknesses (a) $t_s = 1$ nm, (b) $t_s = 5$ nm, and (c) $t_s = 10$ nm. The volume fraction of soft-magnetic phase is estimated by $V_s = t_s/(t_s + t_h)$.

The coercivity $H_c$ and the maximum magnetic energy product versus $V_s$, derived from the data shown in Fig. 2, are presented in Fig. 3. As seen from Fig. 3(a), except in the case of $V_s = 10\%$, the coercivity decreases monotonously with $V_s$ increasing. In the cases of $t_s = 5$ nm and $t_s = 10$ nm, a part of the hard-magnetic phase switches after passing the coercive field at $V_s = 10\%$, which results in an extraordinarily low coercivity. Although the trade-off between the remanence and coercivity in any such two-phase nanocomposite is inevitable, the $(BH)_{max}$ still increases with $V_s$ increasing when $t_s = 1$ nm (lower than the Bloch wall width of the hard-magnetic phase, i.e., 2.6 nm[18]), by effective utilization of the high coercivity of the hard magnetic phase and the high saturation magnetization of the soft-magnetic phase. Such an exchange-coupling principle could provide a way for developing the new generation of permanent magnets. When $t_s = 5$ nm (slightly larger than the Bloch wall width of the hard-magnetic phase), the $(BH)_{max}$ also increases with $V_s$ increasing, which implies that the exchange-coupling effect can still provide a positive contribution to the $(BH)_{max}$. However, as $t_s$ further increases up to 10 nm, the $(BH)_{max}$ decreases with $V_s$ increasing, which indicates that the method of using exchange-coupling to improve the magnetic energy product fails. It is inferred from the above results that the size of the soft-magnetic phase or inhomogeneities plays a crucial role in whether it provides a positive contribution to $(BH)_{max}$ or not. The exchange-coupling principle mentioned above has been well proved through experiments in thin films.[14]

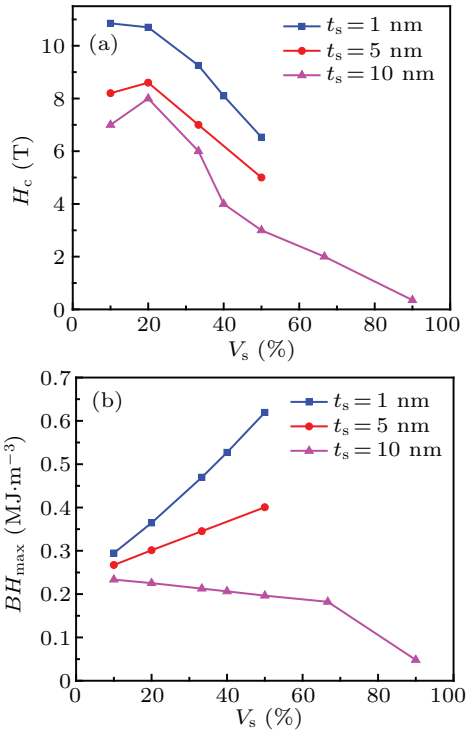



**Fig. 3.** (a) Coercivity $H_c$, and (b) the maximum magnetic energy product $(BH)_{max}$ versus volume fraction of the soft-magnetic phase $V_s$.

To gain an in-depth understanding of the effect of $t_s$ on the magnetic properties, we have systematically investigated the magnetic structure evolution during demagnetization. The magnetization structures with different thicknesses of the soft-magnetic layer at $V_s = 50\%$ are shown in Fig. 4. As can be seen, the magnetic reversal exhibit three different characteristics, depending on the thickness of the soft-magnetic layer. The magnetization in hard-magnetic layers reversal coherent with the soft-magnetic layers when $t_s = 1$ nm is shown in Fig. 4(a). While the magnetization reversal starts at the soft-

magnetic surface layer, and then propagation into the hard-magnetic layers when $t_s = 5$ nm and $t_s = 10$ nm. The main difference between the two cases of $t_s = 5$ nm and $t_s = 10$ nm is that the deflect directions (clockwise or counterclockwise) of magnetic moment in the interior soft-magnetic layer (soft-magnetic layer enclosed by hard-magnetic layers) is consistent with the surface soft-magnetic layer for $t_s = 5$ nm, while the direction of magnetic moment deflection at the surface soft magnetic layer and the interior soft-magnetic layer is different for $t_s = 10$ nm. This is because the soft-magnetic layers are simultaneously affected by the external field and the stray field of the surrounded magnetic layers.[38] Therefore, the magnetization reversal is not only affected by the size of the soft-magnetic phase but also depends on its surroundings.

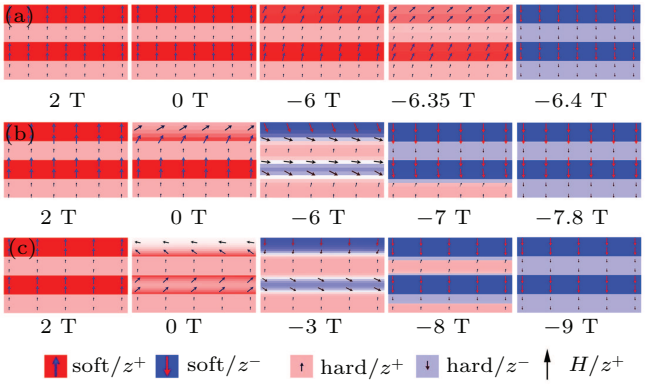



**Fig. 4.** Magnetic structure evolution during demagnetization of the multilayer structure with different thicknesses of soft-magnetic phase, (a) $t_s = 1$ nm, (b) $t_s = 5$ nm, and (c) $t_s = 10$ nm. The volume fraction of the soft-magnetic phase is 50%. The observation plane is parallel to the applied field.

The rotation angle $\theta$ of the central magnetic moment in different layers during demagnetization is shown as a function of the applied field in Fig. 5. Here, the $m_s^{sur}$ and $m_s^{int}$ represent the central magnetic moment of the surface and interior soft magnetic layer respectively, and the $m_h^{sur}$ and $m_h^{int}$ represent the central magnetic moments of the surface and interior hard magnetic layers respectively. It should be noted that the case of $V_s = 50\%$ is selected for a comprehensive investigation because the distances from $m_s^{sur}$ and $m_h^{sur}$ to the surface are the same, which may guarantee a negligible effect caused by the stray field. Based on the existence of qualitatively different magnetization reversal modes as shown in Fig. 5, three exchange coupling phases could be defined. The first one is the exchange-coupled phase. As shown in Fig. 5(a), the $\theta$–$H$ curves of the four magnetic moments are in general overlapped, indicating that there is complete exchange coupling when the soft magnetic layers are thinner than approximately the hard Bloch wall width (2.6 nm for $SmCo_5$). The magnetization reversal mode (synchronous rotation) is quite similar to the behavior of the homogeneous hard magnetic bulk material. The second one is the semi-coupled phase. For thicknesses of soft magnetic layers slightly larger than the Bloch wall width of the hard-magnetic phase, the magnetization reversal mode is dominated by inhomogeneous rotation (Fig. 5(b)). However, although the soft-magnetic phase can be seen, the demagnetization curve is still a single-phase curve owing to the exchange coupling. There is still a collective reversal process, and the forced demagnetization in soft magnetic layers will accelerate the demagnetization of the whole magnet. The last one is decoupled phase. If the soft magnetic layers are much thicker than the hard Bloch wall width, asynchronous rotation as the magnetization reversal mode takes place independently in the soft magnetic layers and the hard-magnetic layers (Fig. 5(c)). Under this condition, the exchange coupling between the hard-magnetic layers is much reduced. In other words, the hard-magnetic layers are separated by the soft magnetic layers, and the forced magnetization reversal at some point cannot spread throughout the whole magnet. Thus, the soft layers guarantee the magnetic decoupling of the individual hard magnetic layers.

The soft magnetic layer can be regarded as a planar soft defect, which is normally present in single-phase hard magnetic materials. Thus, the result of this investigation can be applied to the interpretation of the magnetic properties of both exchange-coupled nanocrystalline composites and inhomogeneous single-phase magnets. As mentioned above, it can be advantageous to have a certain volume fraction impurity with higher saturation magnetization (such as Fe, Co, and their alloys) in a magnet, the magnetic energy product of the system is increased with the volume fraction of the impurities. However, all inhomogeneities should be restricted to the areas smaller than the Bloch wall width of the hard-magnetic phase. Apart from that, the coercivity should be governed by the properties of the hard-magnetic phase, because the existence of the inhomogeneities always leads to decrease of coercivity. Recently, based on the micromagnetic analyses, a self-pinning coercivity mechanism has been proposed.[24] The inhomogeneities possess two competing effects, nucleation of the reversed domains and pinning of the domain walls. The inhomogeneities can lower the local anisotropy and are responsible for the reduction of the nucleation field (the field at which the original saturated state becomes unstable and some change in the magnetization configuration begins to occur), which is responsible for the formation of the local reverse domains. These domains are pinned at the nucleation centers because of the large difference between the magnetic parameters of the impurities and the main phase until the applied field is larger than the pinning field.[24,39] As demonstrated from the above results, the coercivity mechanism is dominated by nucleation when the soft magnetic layers are thinner than the hard Bloch wall width. As the soft magnetic layer increases, there is a gap between the nucleation field and pinning field, and pinning is the dominant coercivity mechanism. It should be noted that the pinning

effect of surface impurities is much weaker than that of internal (see Fig. 5(b)). Therefore, impurities on the surface of the magnet should be avoided. In reality, there will always be areas with very high demagnetization fields, such as at unavoidable corners and edges of a magnet. In these areas, magnetization reversal will set in at the applied field well below the expected coercivity field. The localized Dy or Tb diffusion in Nd–Fe–B magnets could be one solution to this problem.[40]

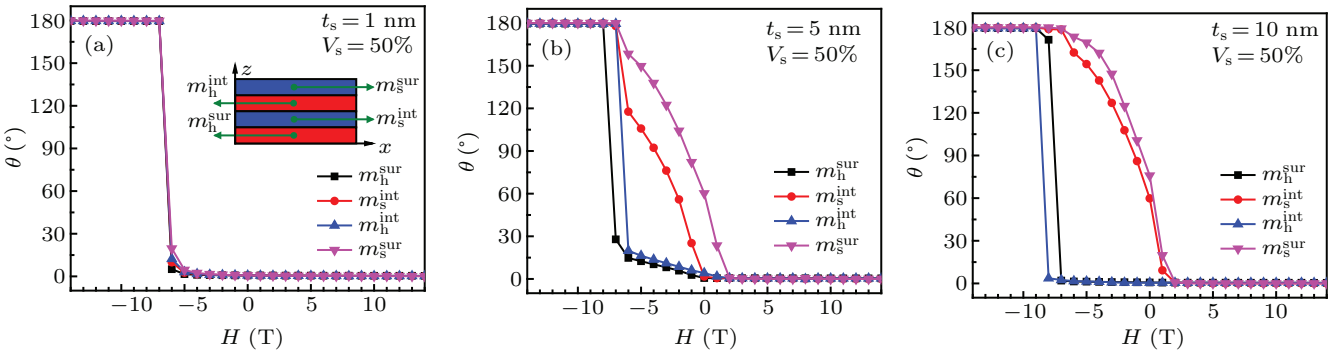



**Fig. 5.** The rotation angle $\theta$ of the central magnetic moment in different layers during demagnetization with different thicknesses of soft-magnetic phase: (a) $t_s = 1$ nm, (b) $t_s = 5$ nm, and (c) $t_s = 10$ nm. The $\theta$ is the angle between the magnetization and the applied field. The volume fraction of the soft-magnetic phase is 50%. The schematic diagram of the selection of the central magnetic moment is inserted in (a).

## 4. Conclusions

In conclusion, we have investigated the effect of size, volume fraction, and surroundings of inhomogeneity on magnetic properties of an inhomogeneous magnetic material via a micromagnetic simulation of a multilayer structure. The inhomogeneities are possible to provide a positive contribution to the magnetic energy product, only when their size is approximately the Bloch wall width of the hard-magnetic phase. The underlying three typical different magnetization reversal modes corresponding to the exchange coupling phase, semi-coupled phase, and decoupled phase dependent on the size of inhomogeneity are revealed. As the thickness of the soft magnetic layer increases, the coercivity mechanism changes from nucleation to pinning. The strategy of reducing the size of inhomogeneities and avoiding the appearance of any inhomogeneities on the surface of magnets should be effective in enhancing the magnetic properties of magnets. The soft magnetic layer can be regarded as a planar soft defect, and thus the present results can be applied to the interpretation of the magnetic properties of both exchange-coupled nanocrystalline composites and inhomogeneous single-phase magnets. The results of the micromagnetic simulation presented in this paper imply certain guidelines for designs of magnetic materials with high performance.

## Acknowledgements

Project supported by the National Key R&D Program of China (Grant No. 2021YFB3500300), the National Natural Science Foundation of China (Grant Nos. 51931007 and 51871005), the Program of Top Disciplines Construction in Beijing (Grant No. PXM2019_014204_500031), the International Research Cooperation Seed Fund of Beijing University of Technology (Grant No. 2021B23), the Key Program of Science and Technology Development Project of Beijing Municipal Education Commission of China (Grant No. KZ202010005009), General Program of Science and Technology Development Project of Beijing Municipal Education Commission (Grant No. KM202010005009), and Chaoyang District Postdoctoral Research Foundation.

## References

[1] Liu X L, Wu X W, Jin J Y, Tao Y M, Wang X H and Yan M 2022 *Rare Met.* **41** 859
[2] Zhang T, Xing W, Chen F, Zhang L and Yu R 2021 *Acta Mater.* **220** 117296
[3] Song X, Ma T, Zhou X, Ye F, Yuan T, Wang J, Yue M, Liu F and Ren X 2021 *Acta Mater.* **202** 290
[4] Wu S, Zhang D T, Yue M, Wang Y Q, Shang Z F, Wu D and Liang J M 2020 *Rare Met.* **39** 250
[5] Zhang T L, Zhang B, Wang H, Jiang C B, Zhang Z H, Wang X Q and Zhang W 2020 *Rare Met.* **39** 70
[6] Lu R B, Ma Z H, Zhang T L and Jiang C B 2019 *Rare Met.* **38** 306
[7] Li X, Lou L, Song W, Huang G, Hou F, Zhang Q, Zhang H T, Xiao J, Wen B and Zhang X 2017 *Adv. Mater.* **29** 1606430
[8] Yang Z, Chen Y, Li Y, Zhang D, Liu W, Lu Q, Wu Q, Zhang H and Yue M 2022 *IEEE Magn. Lett.* **13** 7503205
[9] Lou L, Li Y, Li X, Li H, Li W, Hua Y, Xia W, Zhao Z, Zhang H, Yue M and Zhang X 2021 *Adv. Mater.* **33** 2102800
[10] Wang Y, Yang Z, Wu Q, Liu W, Li Y, Zhang H, Ma X, Cong L, Wang H, Zhang D, Lu Q and Yue M 2022 *Mater. Char.* **187** 111861
[11] Leineweber T and Kronmüller H 1997 *J. Magn. Magn. Mater.* **176** 145
[12] Huang Q, Jiang Q, Shi Y, Rehman S U, Wei X, Li Z, Shi D, Xu D and Zhong Z 2021 *J. Alloys Compd.* **894** 162418
[13] Liu Z, He J, Zhou Q, Huang Y and Jiang Q 2022 *J. Mater. Sci. Technol.* **98** 51
[14] Coey J 2020 *Engineering* **6** 119
[15] Li X, Lou L, Song W, Zhang Q, Huang G, Hua Y, Zhang H T, Xiao J, Wen B and Zhang X 2017 *Nano Lett.* **17** 2985
[16] Leineweber T and Kronmüller H 1997 *Phys. Stat. Sol. (b)* **201** 291
[17] Mohapatra J, Xing M, Elkins J, Beatty J and Liu J P 2021 *Adv. Funct. Mater.* **31** 2010157
[18] Coey J M D 2010 *Magnetism and Magnetic Materials* (Cambridge: Cambridge University Press)
[19] Zhao L, He J, Li W, Liu X, Zhang J, Wen L, Zhang Z, Hu J, Zhang J, Liao X, Xu K, Fan W, Song W, Yu H, Zhong X, Liu Z and Zhang X 2021 *Adv. Funct. Mater.* **32** 2109529
[20] Hubert A and Schäfer R 1998 *Magnetic Domains Magnetic Domains: The Analysis of Magnetic Microstructures* (Berlin: Springer)
[21] Li Z H, Li X and Lu W 2019 *Chin. Phys. B* **28** 077504

[22] Xu X T, Moses A J, Hall J P, Williams P I and Jenkins K 2011 *IEEE Trans. Magn.* **47** 3531
[23] Weng X J, Zhao G P, Tang H, Shen L C and Xiao Y 2020 *Rare Met.* **39** 22
[24] Zhao G P, Zhao L, Shen L C, Zou J and Qiu L 2019 *Chin. Phys. B* **28** 077505
[25] Zhao G P and Wang X L 2006 *Phys. Rev. B* **74** 012409
[26] Li H N, Fan Z W, Li J X, Hu Y and Liu H L 2019 *Chin. Phys. B* **28** 107503
[27] Li L, Dong S, Chen H, Jiang R, Li D, Han R, Zhou D, Zhu M, Li W and Sun W 2019 *Chin. Phys. B* **28** 037502
[28] Zhao Q, He X X, Morvan F J, Zhao G P and Li Z B 2020 *Chin. Phys. B* **29** 037501
[29] Ma X P, Piao H G, Yang L, Kim D H, You C Y and Pan L 2020 *Chin. Phys. B* **29** 097502
[30] Tsukahara H, Iwano K, Ishikawa T, Mitsumata C and Ono K 2019 *Phys. Rev. Appl.* **11** 014010
[31] Sepehri-Amin H, Ohkubo T, Gruber M, Schrefl T and Hono K 2014 *Scripta Mater.* **89** 29
[32] Thielsch J, Suess D, Schultz L and Gutfleisch O 2013 *J. Appl. Phys.* **114** 223909
[33] Oikawa T, Yokota H, Ohkubo T and Hono K 2016 *AIP Adv.* **6** 056006
[34] Donahue M J and Porter D G 1999 *OOMMF User's Guide*, Version 1.0, Interagency Report No. NISTIR 6376
[35] Miltat J E and Donahue M J 2007 *Numerical micromagnetics: Finite difference methods handbook of magnetism and advanced magnetic materials* (John Wiley & Sons, Ltd) pp. 742–764
[36] Rong C B, Zhang H W, Chen R J, Shen B G and He S L 2006 *J. Appl. Phys.* **100** 123913
[37] He Y, Adler P, Schneider S, Soldatov I, Mu Q, Borrmann H, Schnelle W, Schaefer R, Rellinghaus B, Fecher G H and Felser C 2021 *Adv. Funct. Mater.* **32** 2107513
[38] Yang Z, Chen Y, Liu W, Wang Y, Li Y, Zhang D, Lu Q, Wu Q, Zhang H and Yue M 2022 *Nanomaterials* **12** 1261
[39] Li Y, Teng Y, Xu X, Zhang Y and Yue M 2021 *J. Magn. Magn. Mater.* **538** 168261
[40] Liu Z, He J and Ramanujan R V 2021 *Mater. Design* **209** 110004